Pacific Northwest
NATIONAL LABORATORY

Sea Ice Collision Risk Assessment for Tidal Turbine Siting in Cook Inlet, Alaska

November 2021

Ruth Branch
Taiping Wang
Jonathan Whiting

Zhaoqing Yang
Gabriel García-Medina

U.S. DEPARTMENT OF
ENERGY

DISCLAIMER

This report was prepared as an account of work sponsored by an agency of the United States Government. Neither the United States Government nor any agency thereof, nor Battelle Memorial Institute, nor any of their employees, makes **any warranty, express or implied, or assumes any legal liability or responsibility for the accuracy, completeness, or usefulness of any information, apparatus, product, or process disclosed, or represents that its use would not infringe privately owned rights**. Reference herein to any specific commercial product, process, or service by trade name, trademark, manufacturer, or otherwise does not necessarily constitute or imply its endorsement, recommendation, or favoring by the United States Government or any agency thereof, or Battelle Memorial Institute. The views and opinions of authors expressed herein do not necessarily state or reflect those of the United States Government or any agency thereof.

Sea Ice Collision Risk Assessment for Tidal Turbine Siting in Cook Inlet, Alaska

November 2021

Ruth Branch
Taiping Wang
Jonathan Whiting

Zhaoqing Yang
Gabriel García-Medina

Executive Summary

Cook Inlet has great potential for tidal stream energy development. However, the presence of drifting sea ice could create hazardous collision risks for tidal turbine farms. Before turbines can be installed in Cook Inlet, sites must be surveyed to determine how often sea ice is present, how fast it will be moved by the current, and where the trajectories of drifting sea ice will be concentrated. In this study, we assess the collision risk of drifting sea ice for a tidal turbine farm in Cook Inlet using a methodology that combines three elements: 1) remotely sensed data to characterize the seasonal sea ice conditions, 2) a hydrodynamic model to map the water velocities, and 3) a particle tracking model to simulate the drifting sea ice trajectories.

Sea ice conditions in Cook Inlet were mapped with 3.125 km resolution sea ice concentration data from a spaceborne microwave radiometer. Microwaves penetrate through clouds, which enables sea ice concentration measurements regardless of the weather. Monthly maps of average and maximum sea ice concentrations were produced from five years of daily data. The average sea ice concentration maps showed that February is the month with the most sea ice coverage and the maximum sea ice concentration maps showed January, February, and March as all having the possibility of sea ice coverage from upper Cook Inlet south to 60°N. December, April, and May all showed coastal sea ice but less ice in the middle of the inlet. Almost no sea ice was present in Cook Inlet from June until November.

The hydrodynamic model mapped the current speeds in Cook Inlet and was used as input to the particle trajectory tracking model. The highest average current speeds were identified in the Forelands area off the coast of Nikiski, due to the narrow channel. The particle trajectory tracking model showed that many particles transit through the Forelands area closer to the western shoreline than the eastern shoreline. Collision risk maps generated from the particle trajectory maps showed a narrow track near the western shoreline where many particles traveled and the collision risk was high. The collision risk maps were further refined by discarding locations where the sea ice concentration was below 30% in the period of analysis. A final map combines information from the current speed distribution predicted by the hydrodynamic model, the sea ice concentration analysis, and the particle trajectory tracking model. The collision risk map shows there are areas near the eastern shoreline that have high current speeds but lower collision risks than near the western shoreline. The resulting map will enable tidal energy developers to identify the best locations for the deployment of tidal turbines and other offshore platforms in Cook Inlet.

Acronyms and Abbreviations

ADCP	Acoustic Doppler Current Profiler
CFSv2	Coupled Forecast System version 2
FVCOM	Finite-Volume Community Ocean Model
GCOM	Global Change Observation Mission
GNOME	General NOAA Operational Modeling Environment
GSFC	Goddard Space Flight Center
NASA	National Aeronautics and Space Administration
NCEP	National Centers for Environmental Prediction
NOAA	National Oceanic and Atmospheric Administration

Acknowledgments

Contents

Figures

Tables

1.0   Introduction

Cook Inlet, Alaska, has enormous tidal power potential (Kilcher et al. 2016), but the locations in the inlet that have high tidal current speeds are also affected by seasonal sea ice, which creates hazardous collision risks for ships and offshore structures. Figure 1 shows a satellite image of sea ice in Cook Inlet on January 15, 2020. where ice can be seen in Knik Arm, Turnigain Arm, near Anchorage and extending down south of the Forelands region. Damage to ships and docks has been documented at several locations in Cook Inlet and several incidents are listed in Table 1 (Mulherin et al. 2001; Parker and Jacobs 2018). Sea ice presents risks to all offshore structures (Sanderson and Redden 2015; Huang et al. 2021) and needs to be mapped before developers can choose the best installation sites.
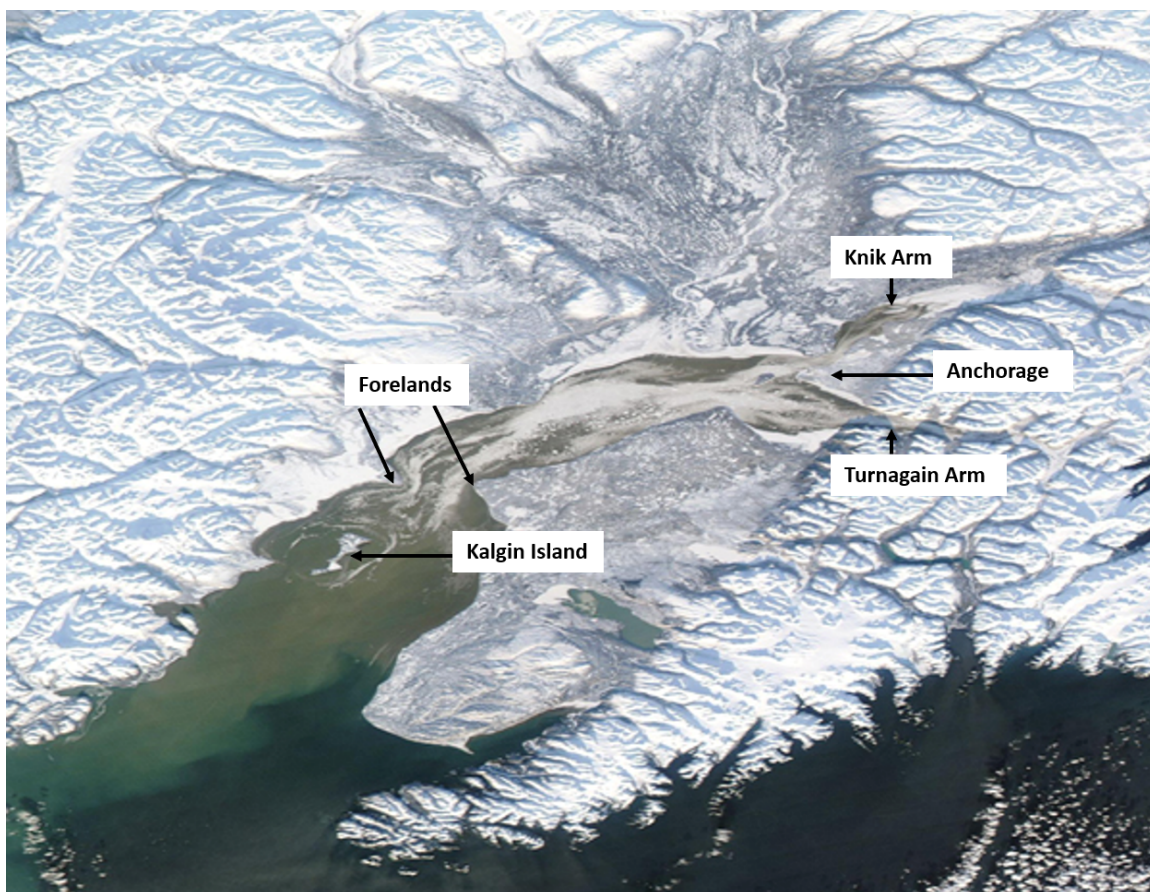
Figure 1.   Sea ice in Cook Inlet on January 15, 2020. The locations of Knik Arm, Anchorage,Turnagain Arm, and the Forelands region are noted for reference. (Image Credit: MODIS Land Rapid Response Team, NASA GSFC.)

Table 1.   Vessel and structure damage in Cook Inlet caused by floating ice. Data from
             (Mulherin et al. 2001; Parker and Jacobs 2018)

Location	Damage	Cause of Accident
Port of Anchorage	Pilings torn from dock, $33,000	Winter ice and tide
Knik Arm Shoal	Tanker *Evje IV* ruptured cargo of oil tanks after striking shoal	Winter ice ripped out marker buoy
Port of Anchorage	540-ft SS *Philadelphia* stuck object, $300,000	Ice pan pushed ship into obstacle
Fire Island Shoal	497-ft SS *Newark* grounded	Heavy ice and tide
Port of Anchorage	523-ft SS *Galveston* came loose when ice severed mooring lines	Ice floe and tide
Anchorage City Dock	540-ft SS *Philadelphia* collided with dock, $14,000	Large ice pan forced ship into dock
Nikiski	T/V *Seabulk Pride* broke free and grounded on opposite shore	Ice accumulation broke the mooring

2.0 Methods

Remotely sensed sea ice data are combined with a hydrodynamic circulation model, wind data, and a trajectory model to map the sea ice collision risk in Cook Inlet, Alaska. The sea ice conditions in Cook Inlet are characterized by producing maps of the monthly maximum and average sea ice concentrations. A circulation model is used to model the hydrodynamics, and a trajectory model uses those water velocities and wind data to predict where ice floes are most likely to move due to the currents and wind. The resulting maps of sea ice concentrations and simulated trajectories are combined to produce collision risk maps. The collision risk maps are compared to the average current speed map to determine the best locations with high current speeds and low collision risks for turbine installations.

2.1 Sea Ice Concentration

Sea ice concentration data were obtained from the Advanced Microwave Scanning Radiometer 2 (AMSR-2) instrument, which is flown on the GCOM-W1 satellite. Microwave sensors can detect sea ice through clouds, which means sea ice concentration data are available every day regardless of the weather. The AMSR-2 data were processed into sea ice concentration values from Level-1R brightness temperature measurements (Kaleschke et al. 2001; Beitsch et al. 2014). The gridded 3.125 km resolution data were downloaded from the University of Hamburg's Integrated Climate Data Center (ftp://ftp-projects.cen.uni-hamburg.de/seaice/AMSR2/3.125km/). Daily sea ice concentration data were downloaded for five years from 2016 to 2020 and analyzed to produce maps of the monthly average and maximum sea ice concentration in Cook Inlet.

2.2 Hydrodynamic Circulation Model, FVCOM

The hydrodynamic circulation in Cook Inlet was modeled using the unstructured grid Finite Volume Community Ocean Model (FVCOM) (Chen et al. 2003, 2006). In this implementation of FVCOM, the water surface elevation and velocities throughout the water column are simulated after using the external forcing of open boundary tidal elevations and wind. River flow and surface gravity waves were not used as forcings or modeled in this implementation. The bathymetry was interpolated to the model grid from NOAA's 50 m resolution Cook Inlet bathymetry data set. The model grid had approximately 199,000 nodes and 392,000 elements with varying spatial resolutions from 90 m to 1000 m. Cook Inlet has a deep channel in the Forelands region (Figure 2) and the node spacing is dense there to resolve the water velocities with high resolution. Ten uniform sigma layers were used in the vertical direction and the model was forced with tidal elevation time series with 13 major harmonic constituents. The model was run in barotropic mode, which does not take into account the effect of water density variations caused by salinity and temperature gradients. Current and water level data were used for model validation. The current and water level data were collected by NOAA at six ADCP moorings and three tide gauges. The model was run for 35 days, from November 25, 2017, to January 1, 2018. The November output was considered the spin-up time and the December output was used to force the trajectory model. The details of the FVCOM model configuration and validation are given by Wang and Yang (2020).
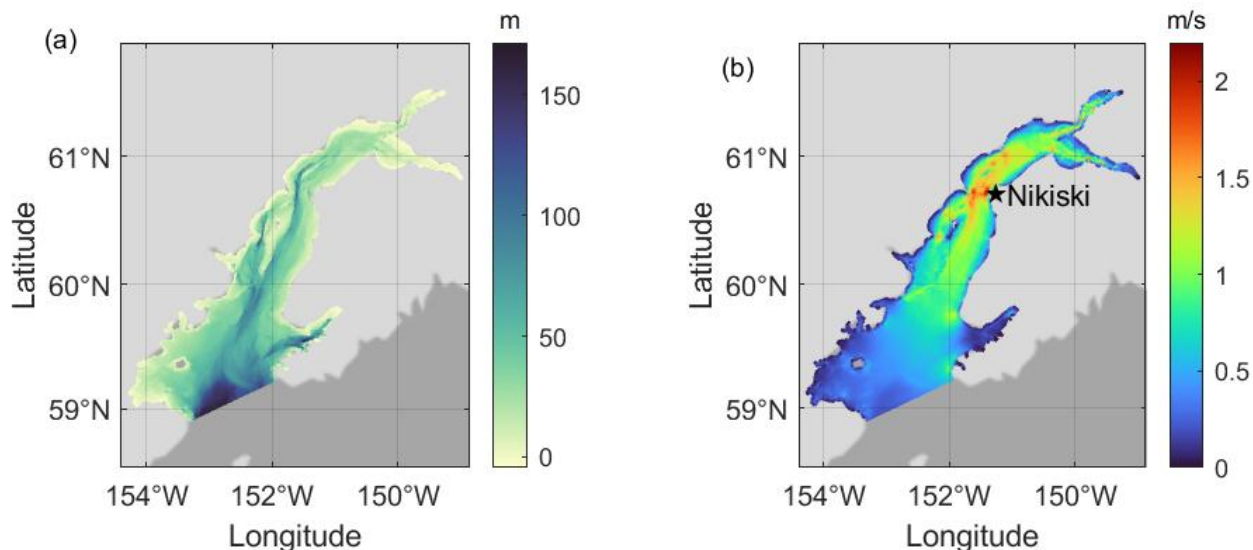
Figure 2.   Cook Inlet (a) bathymetry, (b) depth, and time averaged current speeds as calculated by FVCOM. Nikiski is the town on the eastern shore of the Forelands region.

The FVCOM output that is used to force the trajectory model shows strong tidal current speeds in the Forelands area off the coast of Nikiski (Figure 2b). The depth-averaged current speed offshore of Nikiski is up to 3 m/s and the tidal range is up to 8 meters during spring tide (Figure 3 a and b). The tides have strong diurnal inequality at this location and significant differences in the current speeds and water levels during spring and neap tides. The neap tides have maximum current speeds of 2.5 m/s and a tidal range of 6 m.
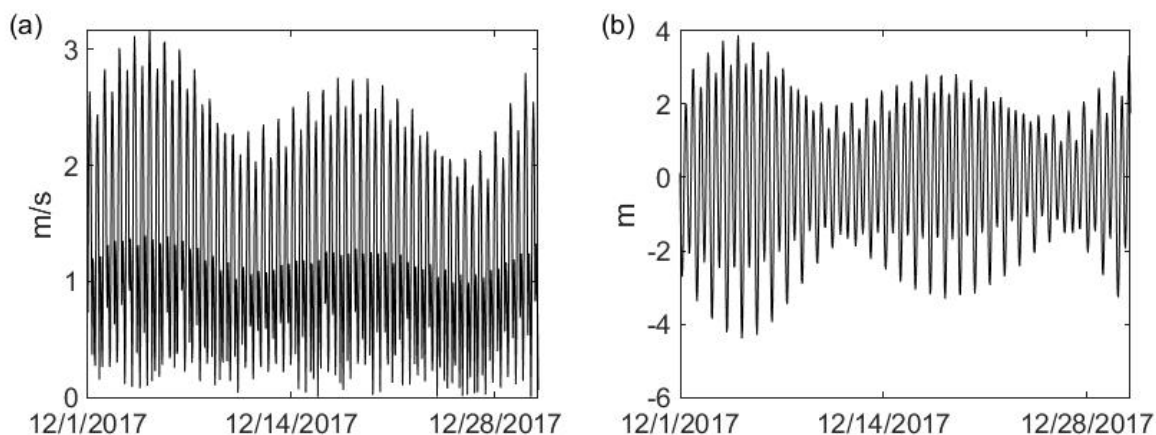
Figure 3. FVCOM output offshore of Nikiski. (a) Depth-averaged current speed.(b) Water level.

2.3   Trajectory Model, GNOME

Sea ice trajectories were calculated using the General NOAA Operational Modeling Environment, GNOME. GNOME is a trajectory model developed by NOAA's Office of Response and Restoration to track oil spills (Beegle-Krause 1999). It is used operationally in the U.S. to

guide the emergency response after a spill. In this study it was run in Python using the PyGNOME utilities and bindings (https://gnome.orr.noaa.gov/doc/pygnome/index.html).

GNOME uses inputs of current and wind to predict where surface particles such as oil or sea ice will travel. In this study it was forced with FVCOM currents and wind data from the Climate Forecast System Version 2, CFSv2, (https://rda.ucar.edu/). The wind data from a height of 10 m had 0.2°resolution and was available at hourly time steps. Besides the wind and current forcing, GNOME has several adjustable parameters that control how the wind and currents move the particles. The windage controls how much the wind moves the particles. For these tests, the windage of the ice particles was set at 0.03. This number was determined by previous researchers who tracked debris from the 2011 tsunami in Japan (NOAA 2013; Maximenko et al. 2018). The exact windage value of sea ice in Cook Inlet is not known, but it would be similar to tsunami debris that has some surface area above the water. Oil spills would have a different windage because oil does not protrude from the surface at all. The diffusion coefficient determines how much each particle randomly moves at each time step. There are several methods for calculating diffusion, but for this study we used Random Walk and the value was set at 5000.

Particle tracking simulations were run for 14 days and the particle location was calculated every 15 minutes, but only output every hour. For the collision risk assessment, the particles were released on an evenly distributed grid with points separated by 3.125 km (Figure 4). The grid locations were chosen because they are the same locations as sea ice concentration measurements. Some of the particle release locations were on land but they are disregarded during the trajectory tracking.
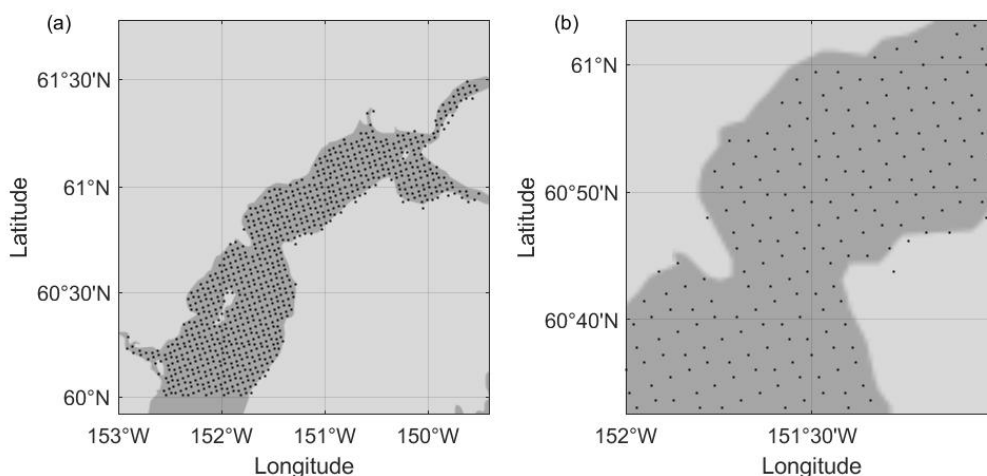
Figure 4. Locations of the sea ice particles released in the GNOME particle tracking model. Point spacing is 3.125 km. (a) Region of particle release (b) zoomed in on the Forelands region.

2.4   Wind Forcing

Wind speed data used to force the trajectory model were the Climate Forecast System version 2, CFSv2, which was obtained from the National Centers for Environmental Prediction (NCEP). The wind speed offshore of Nikiski in the Forelands region is plotted in Figure 5. During the study period the wind was mostly from the north but did reverse for short periods of time. The maximum wind speed was approximately 10 m/s.
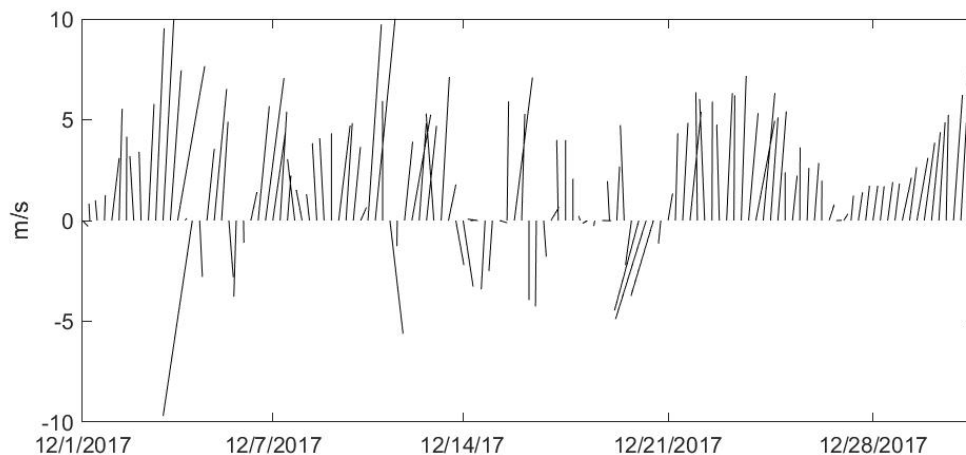
Figure 5.   Wind speed and direction at Nikiski obtained from the Climate Forecast System Version 2, CFSv2. Wind speed is shown as the distance from the x-axis and wind direction is plotted as the direction the wind is coming from. Arrows above the x-axis indicate the wind is from the north and arrows below the x-axis indicate the wind is from the south.

2.5 Particle Trajectory Simulations

Trajectory tracking simulations were conducted with single particle releases and with particles released at multiple locations. Sensitivity simulations were conducted to evaluate the effects of wind and tidal currents on particle trajectories by running GNOME with wind only, currents only, and wind and currents combined. Particles were released during both ebb and flood tide and the 14-day simulations covered a range of tidal conditions. The details of the simulations are listed in Table 2. Runs 1–4 were simulations with a single particle released in a high velocity area offshore of Nikiski to confirm that the particles were moving in the expected directions due to the wind and current forcings. Runs 5–7 were the simulations run to test the release of particles at the 858 points north of 60°N. Run 8 was started during neap flood tide with particles released every hour for six hours at all of the 858 locations north of 60°N. Runs 9, 10, and 11 were the same as Run 8 but started during spring flood, neap ebb, and spring ebb, respectively.

Table 2. Particle Trajectory Simulations

Run	Particles	Wind	Current	Ebb/Flood, Spring/Neap	Tide
1	1	N	Y	E, S	
2	1	Y	Y	E, S	
3	1	N	Y	F, S	
4	1	Y	Y	F, S	
5	858	Y	N	E, S	
6	858	N	Y	E, S	
7	858	Y	Y	E, S	
8	858x6	Y	Y	F, N	
9	858x6	Y	Y	F, S	
10	858x6	Y	Y	E, N	
11	858x6	Y	Y	E, S	

3.0 Results and Discussion

3.1 Sea Ice Conditions

Sea ice begins to form in Cook Inlet in December and can be present until May. It is present along the shoreline of Cook Inlet from December to May but rarely forms in the center below latitude 60°N. No significant amounts of ice are present between June and November. Monthly averages of sea ice concentration show February to be the month with the largest area of sea ice coverage (Figure 6). In January, February, and March, the average sea ice concentration is higher in the center of Cook Inlet near 61°N than it is near the shoreline at the same latitudes. This concentration of ice in the center of Cook Inlet near the Forelands region was also observed in the photograph taken on January 15, 2020, as shown in Figure 1. Maps of the
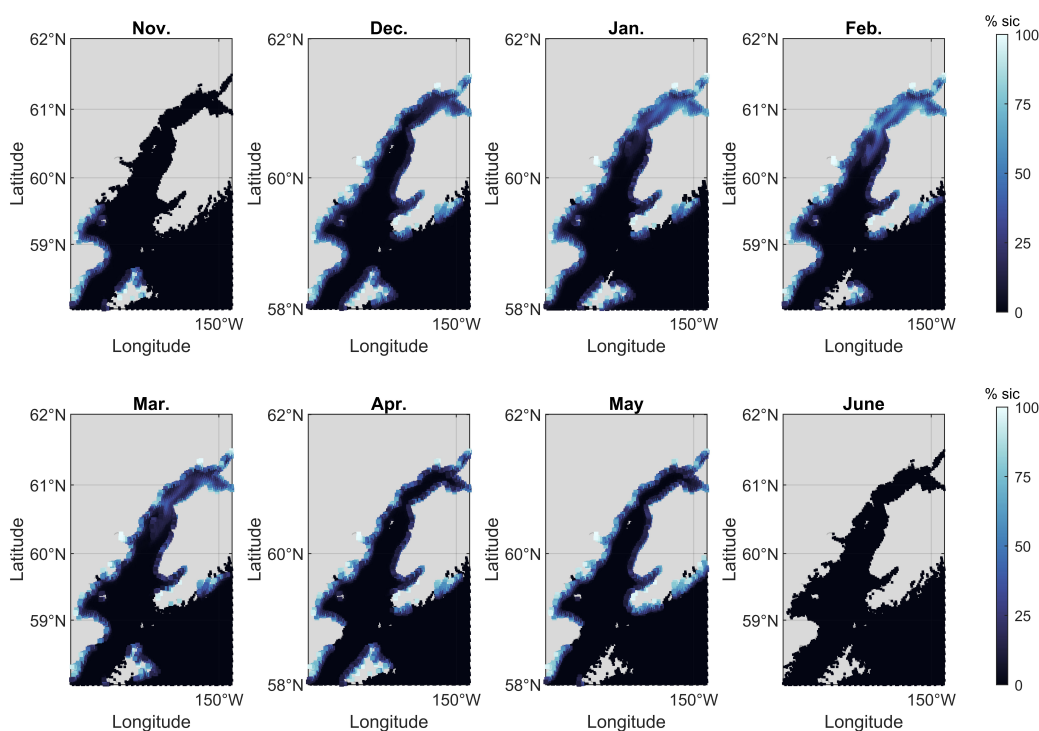
Figure 6.   Monthly average sea ice concentration percentage in Cook Inlet calculated with AMSR2 data from 2016 to 2020.

monthly maximum sea ice concentration at each pixel also show February as the month with the highest concentrations (Figure 7). The quality of sea ice coverage from the AMSR2 data set is good in northern Cook Inlet but not perfectly continuous around the south end and along the Alaska coastline east of the inlet. Holes in the coverage are noticeable in Figure 7 on the eastern coastline of Cook Inlet south of 60°N.
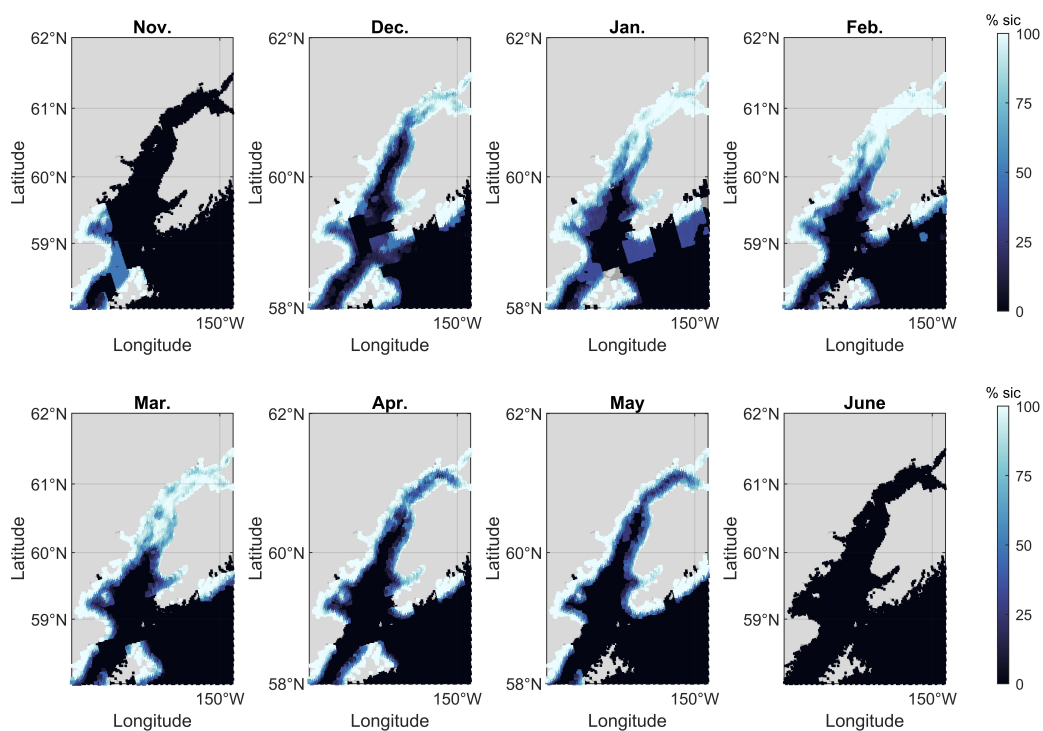
Figure 7. Monthly maximum sea ice concentration percentage in Cook Inlet calculated with AMSR2 data from 2016 to 2020.

3.2   Trajectory Modeling

The trajectory modeling with GNOME was tested by releasing a single particle offshore of Nikiski and tracking it for 14 days to ensure the particle motion was consistent with the wind and tidal current forcing. This release location was chosen because the high current speeds indicate this region may be of interest to turbine developers (Figure 2b). Tests were completed with current only and wind and current. The current only tests were started during ebb tide (Run 1) and flood tide (Run 3). The wind and current tests were started with releases during ebb tide (Run 2) and flood tide (Run 4). The flood tide runs began on December 5, 2017, at 10:00 and the ebb tide runs began at 17:00. Trajectory points far south of latitude 60°N are ignored in the analysis because significant ice concentrations were not found south of latitude 60°N in the five years surveyed for this study (Figure 7). During the ebb tide run with current only (Run 1), the particle initially moved south and then oscillated north and south with the tide changes (Fig. 8a). It drifted eastward and was beached on day seven. The red point on the eastern shoreline indicates the location where it was beached. Run 2, which began on ebb current and also included wind, showed a southward trajectory at first, then a northward trajectory, and finally a southward trajectory that exited the test area on day seven (Fig. 8b). No red points for day 14 are shown on Figure8b because they are south of 60°N. The current only flood tide trajectory (Run 3) propagated northward first and then oscillated north and south with the tide while slowly drifting northwest (Figure 8c). The wind plus current run that was started during flood tide (Run 4) showed a northward trajectory at first and then north-south oscillations that were southeast of the current only trajectory (Figure 8d). This particle beached on day six on the eastern shoreline. These results show that if a particle is released in the Forelands region during ebb, it will travel south with the tidal current and then oscillate north and south but not propagate northward into the upper inlet if the wind conditions are similar to those of this test. If a particle is released in the Forelands region during flood, it will travel north and then oscillate north and south according to the tidal currents. It may propagate south of the Forelands region if the wind is from the north and it does not get beached along the shoreline. The particle motion in these tests showed that the tidal currents caused north to south oscillations and the wind pushed the particle south, which is consistent with the wind direction.
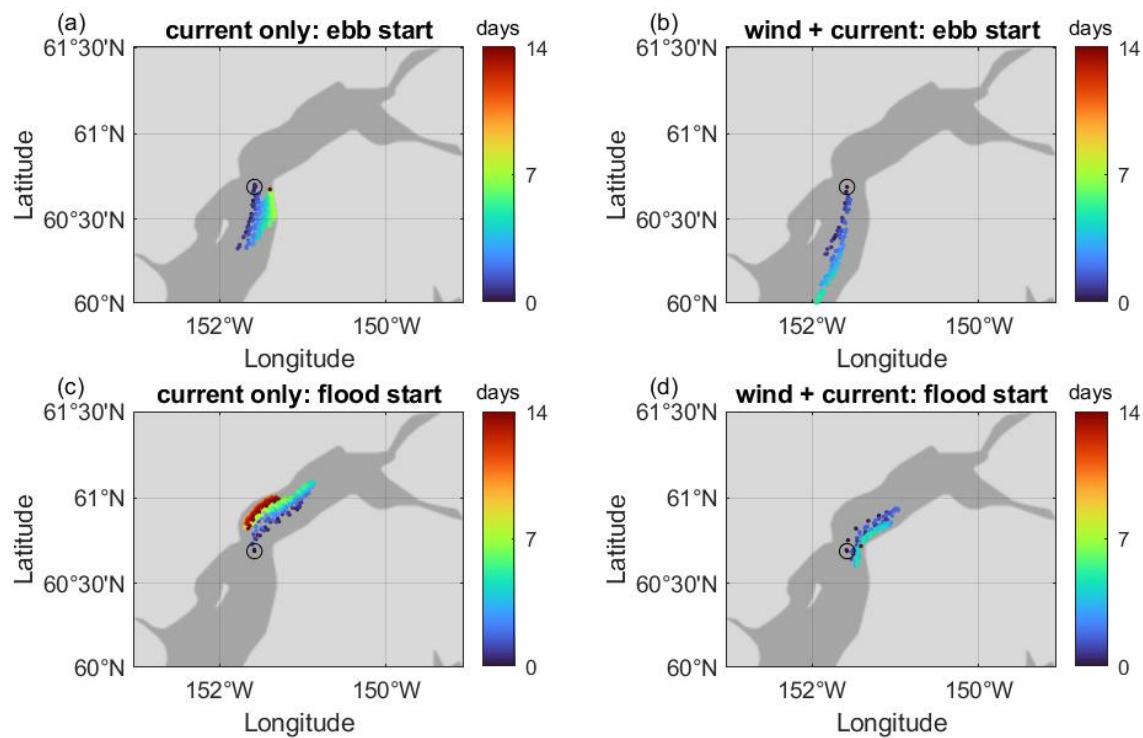
Figure 8.   Fourteen-day trajectories of particles released at the location of the black circle offshore of Nikiski. GNOME was run using (a) Run 1: only current and started on ebb, (b) Run 2: wind and current started on ebb, (c) Run 3: only current started on flood, and (d) Run 4: wind and current started on flood.

3.3 Collision Risk Assessment

Collision risk was assessed by releasing particles at the locations shown in Figure 4, tracking their trajectories with GNOME, and comparing their trajectory locations to sea ice concentration maps. At the end of the GNOME run, each point in the trajectory was compared to the FVCOM grid and the grid point it was closest to was considered to have had a collision. Collisions were summed at each FVCOM grid point and heat maps of the collisions were generated to show the density distribution of particle trajectories. Three sample runs with wind only, current only, and both wind and current demonstrate how the wind and current move the particles on a run started during ebb tide (Figure 9). When GNOME was run with only wind and no current (Run 5), the wind pushed the particles south and at the end of the 14-day simulation the locations with large amounts of collisions were south of 60°N (Figure 9a). South of 60°N is outside the region where sea ice occurs except along the shoreline (Figures 6 and 7). When GNOME was run with only current and no wind (Run 6), there were several areas north of 60°N where particles congregated (Figure 9b). When wind and current were combined (Run 7), most particles were pushed south of 60°N, but as they traveled south many particles transited through a narrow strip in the Forelands region (Figure 9c). The narrow strip in the Forelands region where many collisions occurred was closer to the western shore than to the eastern shore (Figure 9d).
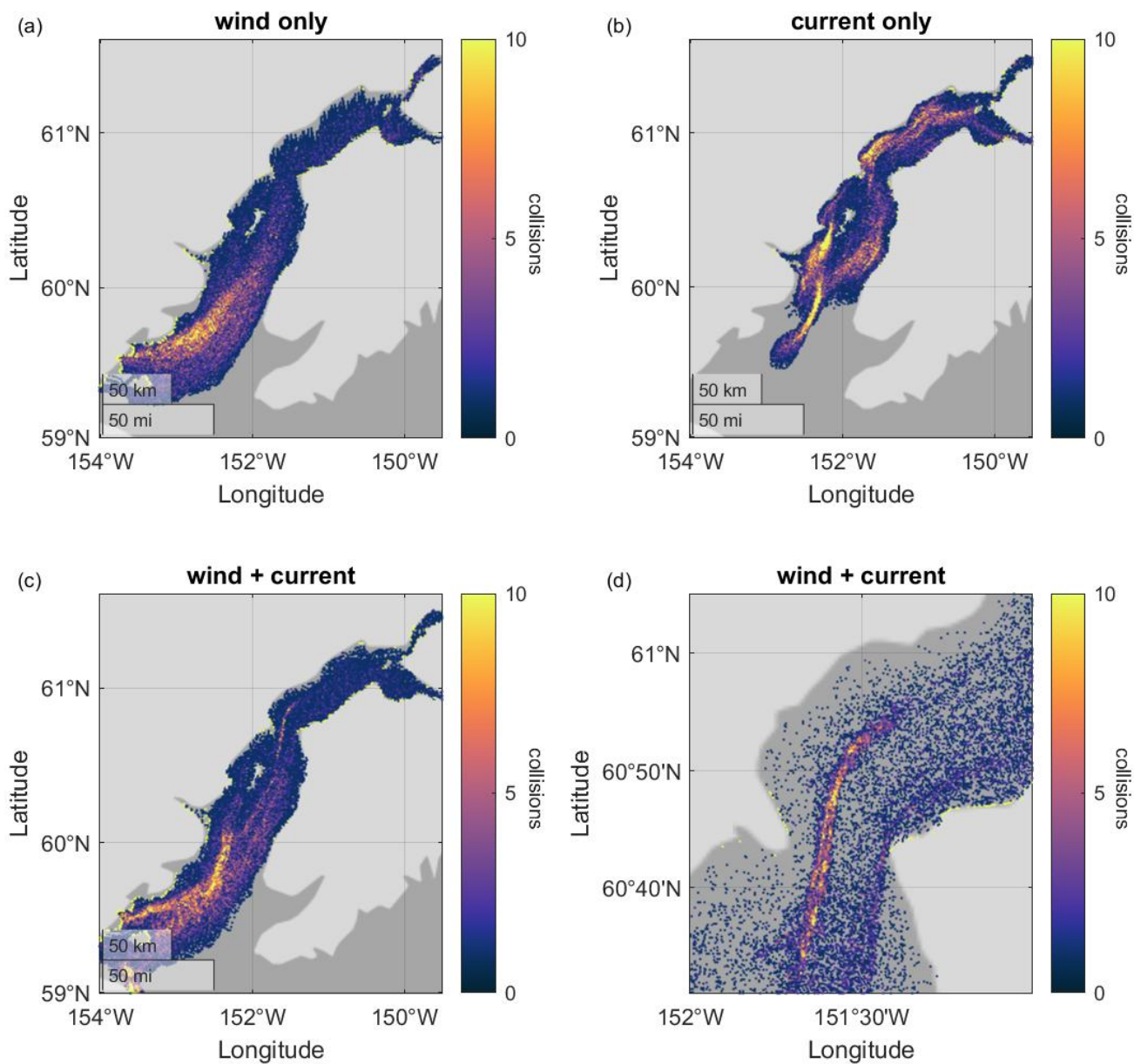
Figure 9.   Collisions during a 14-day simulation after one release of 858 particles at high tide. Release locations are shown in Figure 4a. Simulation run with (a) Run 5: wind only, (b) Run 6: current only, (c) Run 7: wind and current, and d) Run 7: wind and current zoomed in on the Forelands region.

Simulation runs conducted with six hourly particle releases produce statistically robust maps of the collision risk (Figure 10). All simulations were run for 14 days starting at neap flood, spring flood, neap ebb, or spring ebb (Runs 8-11). The locations where GNOME predicts high collision risks coincide with trajectories of drifting buoys in a previous study (Johnson 2008). The Johnson (2008) study did not map the density of drifter trajectories at each location or map collision risks, but the good comparison of the drifter tracks with the GNOME collision risk maps suggests GNOME is accurately predicting particle motion in Cook Inlet.
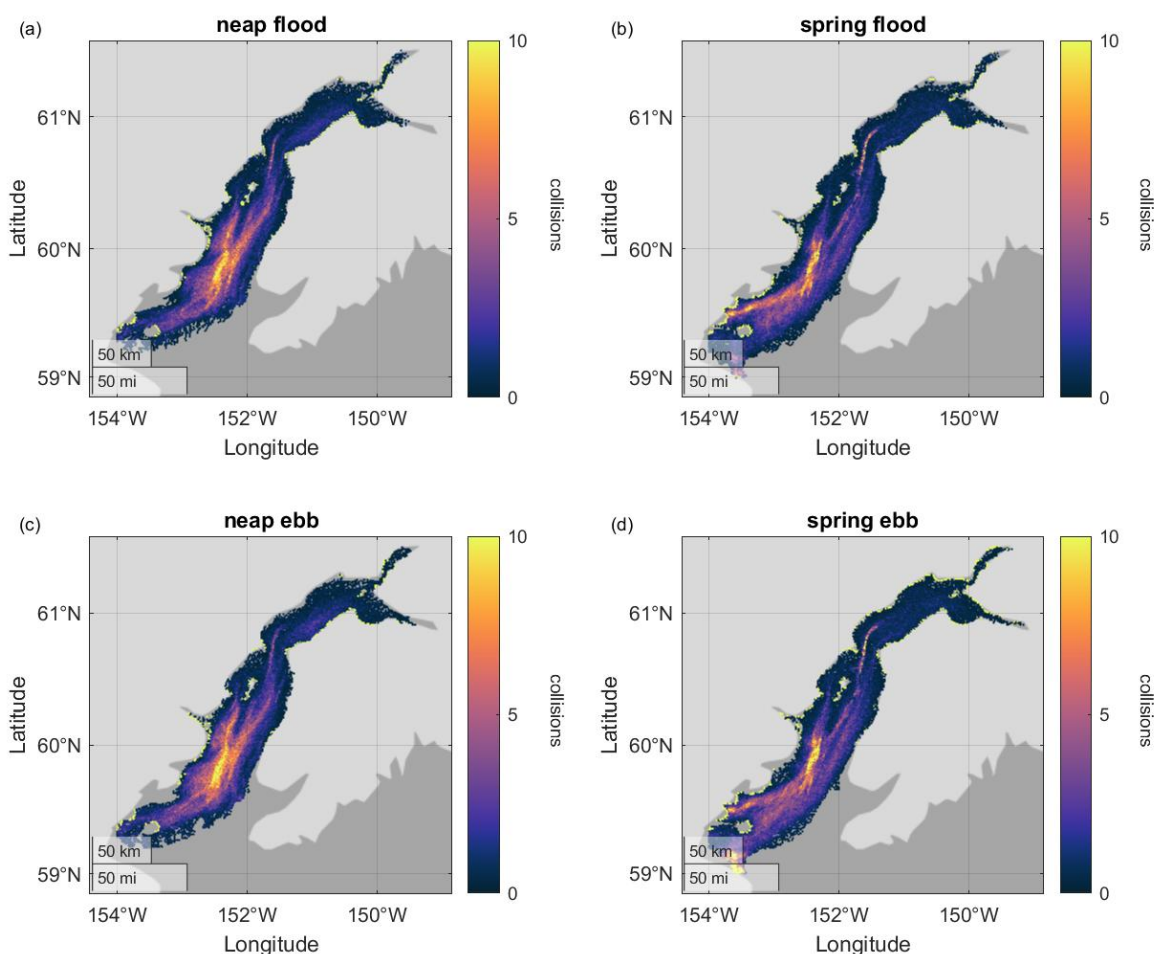
Figure 10.   Collisions in Cook Inlet during 14-day simulations after releasing 858 particles in six runs. Collisions are plotted per release for comparison with Figure 9. Ice released during (a) neap flood (Run 8), (b) spring flood (Run 9), (c) neap ebb (Run 10), and (d) spring ebb (Run 11).

The patterns of the collision risk maps are similar regardless of the time of the trajectory release, except that the collision risk is more concentrated in some regions during the spring tide releases than during the ebb tide releases. All of the maps show high collision risks in the Forelands region, areas southeast and southwest of Kalgin Island, and south of 60°N (Fig. 10). In the Forelands region, the particles tend to travel through a narrow strip in the location of a deep channel (Figures 2a & 10). They are not as concentrated in that area when released

during neap tides as they are when released during spring tides (Figure 11).
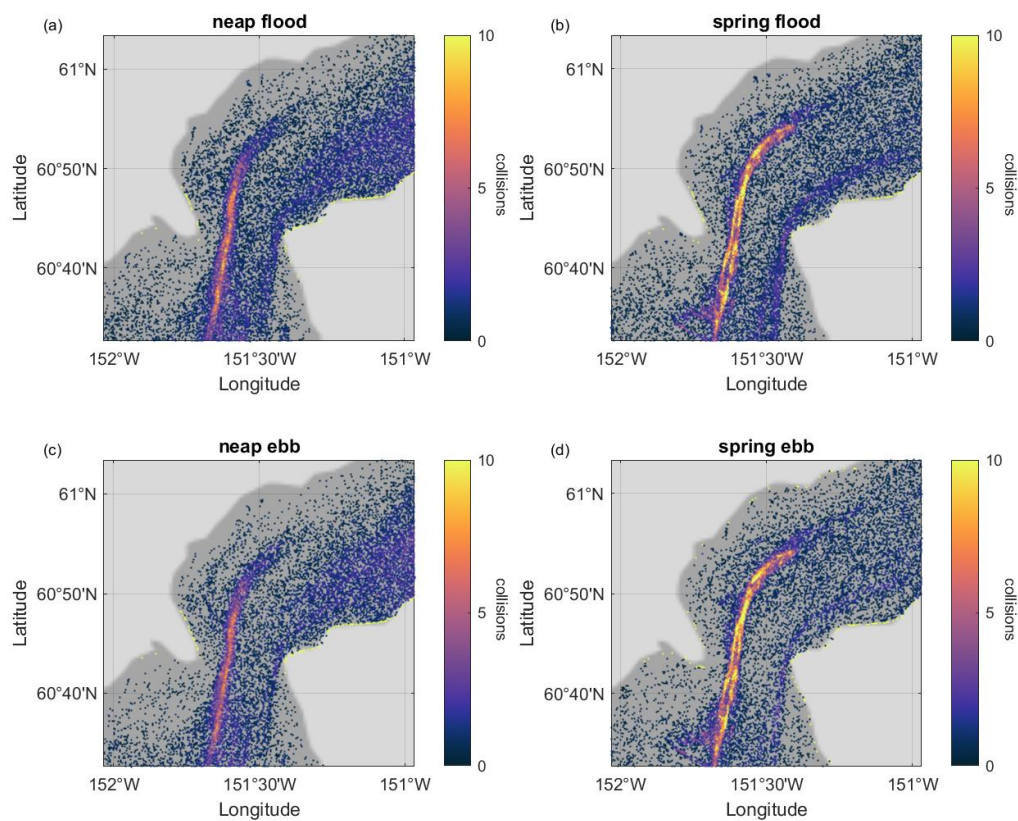

Figure 11.   Collisions in the Forelands region during 14-day simulations after releasing 858 particles in six runs. Collisions are plotted per release for comparison with Figure 9. Ice released during (a) neap flood (Run 8), (b) spring flood (Run 9), (c) neap ebb (Run 10), and (d) spring ebb (Run 11).

The collision risk maps calculated from the GNOME output are applicable for any type of particle such as oil or sea ice. They do not take into account the spatial and temporal characteristics of sea ice concentration in Cook Inlet. To estimate the collision risk due to sea ice, the collision risk maps were refined by combining them with information about sea ice coverage derived from the satellite maps. Figure 12 shows only the collision risk where the average February sea ice concentration is above 30%. February was chosen because it is the month with the most sea ice coverage (Figures 6 and 7). The collision risk in areas affected by sea ice is strongest in the Forelands region for releases during neap flood, spring flood, neap ebb, and spring ebb (Figure 12). The collision risks near the shorelines of the Forelands region are excluded because those areas did not have average sea ice concentrations above 30% in February (Figure 13).
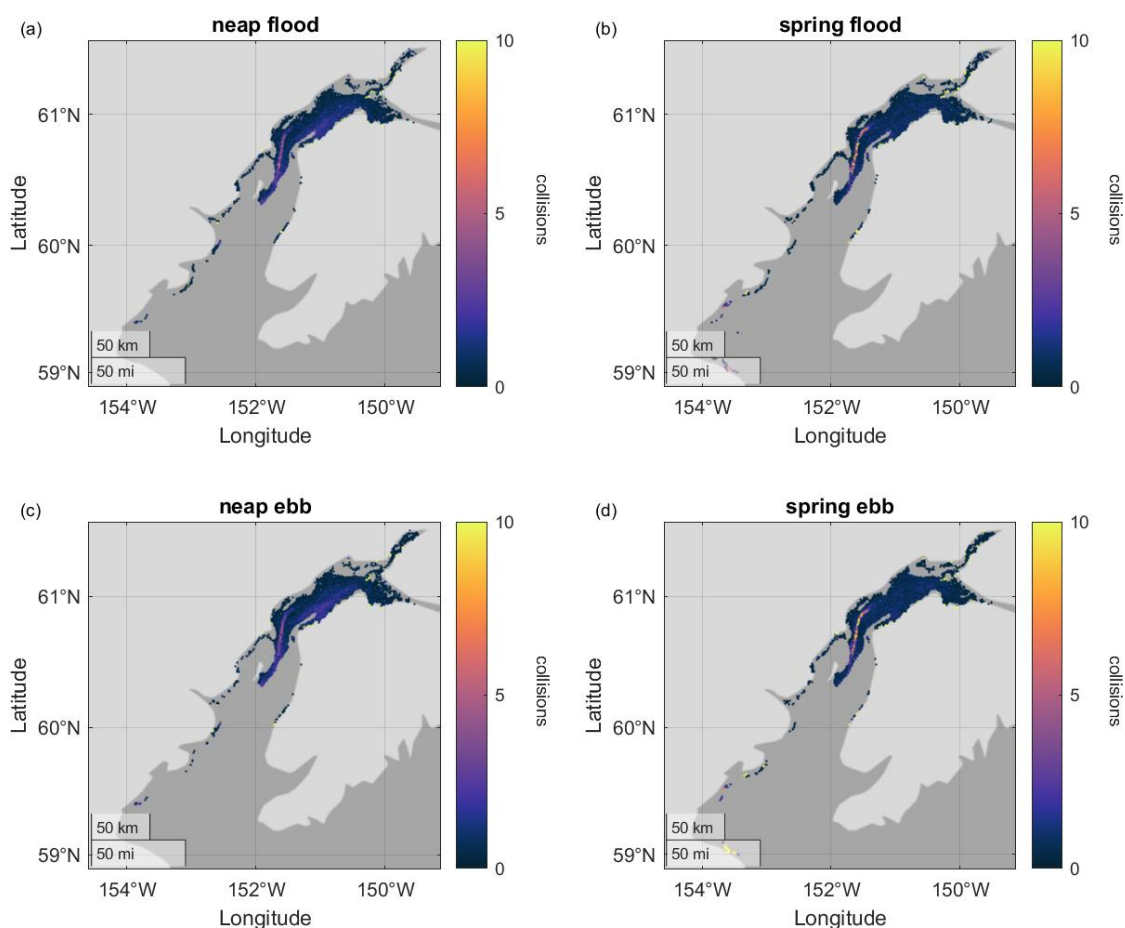
Figure 12.   Sea ice collisions in Cook Inlet after ice was released during (a) neap flood (Run 8), (b) spring flood (Run 9), (c) neap ebb (Run 10), and (d) spring ebb (Run 11). Collisions are plotted per release for comparison with Figure 9. Only locations where the average February sea ice concentration is greater than 30% are shown.
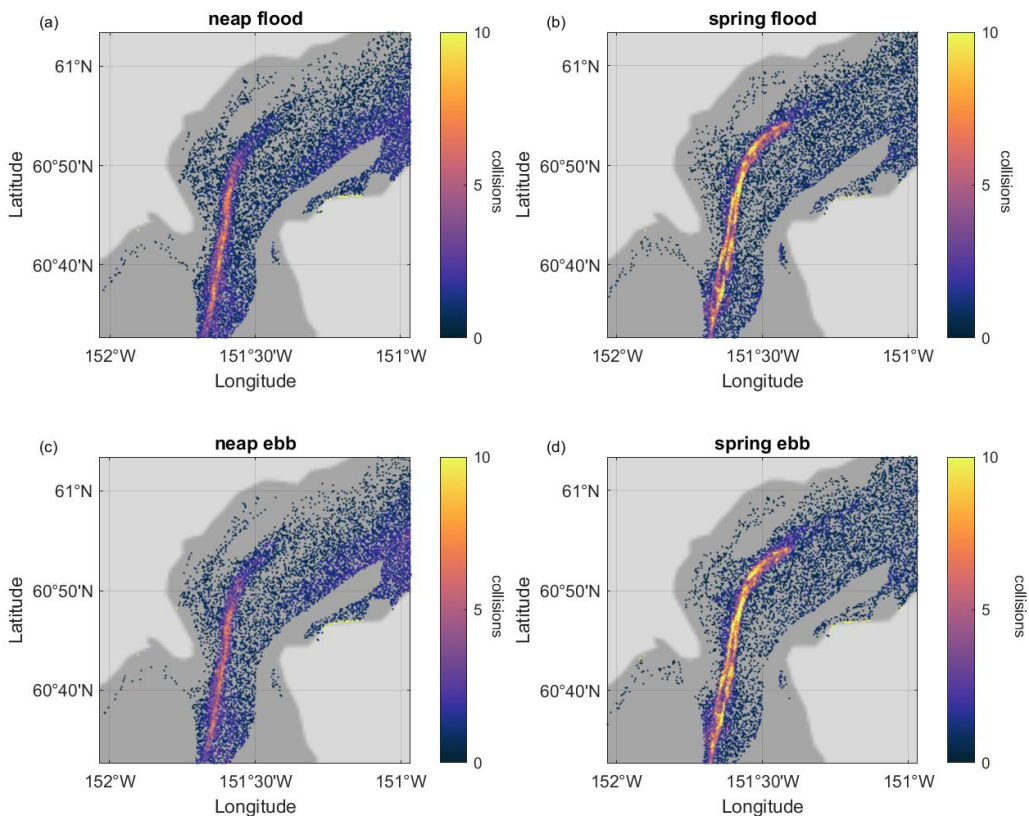
Figure 13. Sea ice collisions in the Forelands region after ice was released during (a) neap flood (Run 8), (b) spring flood (Run 9), (c) neap ebb (Run 10), and (d) spring ebb (Run 11). Collisions are plotted per release for comparison with Figure 9. Only locations where the average February sea ice concentration is greater than 30% are shown.

3.4   Tidal Turbine Siting

One application of the collision risk assessment is to inform turbine siting decisions. Cook Inlet has strong tidal energy resources, but developers need to locate sites with high current speeds and low collision risks. Turbines often require currents above 0.5 m/s to operate and currents above 1.5 m/s are considered a strong resource. Figure 14 shows maps of the depth-averaged and time-averaged current speeds output by FVCOM for a range of speeds. All speeds are shown in Figure 14a and subsets of the speeds are shown in Figure 14b, c and d. Turbine developers who need an average speed of at least 0.5 m/s should choose from a location shown in Figure 14b. As the current speed threshold increases to 1 m/s, the coastal areas do not fit the criteria because the higher current speeds are farther from shore (Figure 14c). The highest current speeds are in the Forelands region, but there are a few high current speed locations farther north in Turnagain Arm and Knik Arm (Figure 14d). The high current speed sites in Turnagain Arm and Knik Arm are not locations with high collision risks, but the Forelands region is an area with high collision risks (Figure 13).

Maps of the Forelands region show the exact locations where FVCOM predicts high current speeds and GNOME predicts high collision risks (Figure 15). High current speeds are found on the eastern shoreline, in the middle of the inlet near latitude 60°45'N, and in the middle of the inlet near 61°N (Figure 15a). The collision risk locations are concentrated in a thin strip in the middle of the channel (Figure 15b). To compare the current speed map directly to the collision risk map, the collision risks were averaged into 0.01° bins. Bins with averages greater than five collisions are shown as black on top of the current speed map in Figure 16. The high collision risk area coincides with an area of high current speeds near the west Foreland area, but there are other areas with high speeds that could be potential turbine sites. Very high tidal current speeds occur near the east Foreland area and this was not identified as a high collision risk location. It is also a good location for a tidal turbine because it is close to the existing electricity grid. The area has low average sea ice concentrations (Figure 6), but the maps of the monthly maximum sea ice concentration show it is susceptible to sea ice formation from December through May (Figure 7). While the monthly average sea ice concentration is a useful parameter for determining which areas are most affected by sea ice, an average monthly sea ice concentration below 30% does not imply that sea ice never forms in those areas, so it could be a collision risk when it is present.
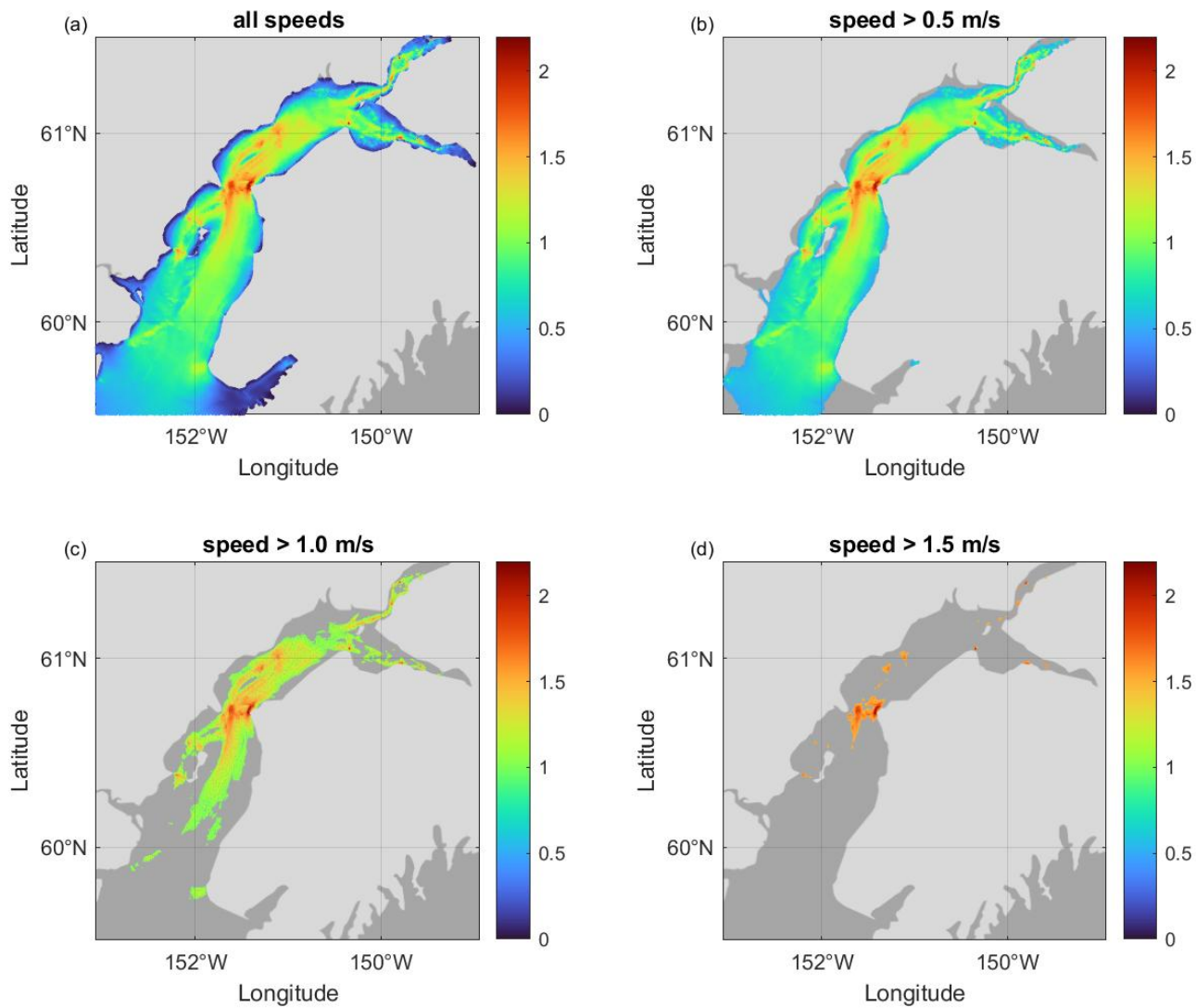
Figure 14.   Depth- and time-averaged current speeds output by the FVCOM model. (a) All speeds, (b) locations where the speed is greater than 0.5 m/s, (c) locations where the speed is greater than 1 m/s, and (d) locations where the speed is greater than 1.5 m/s.
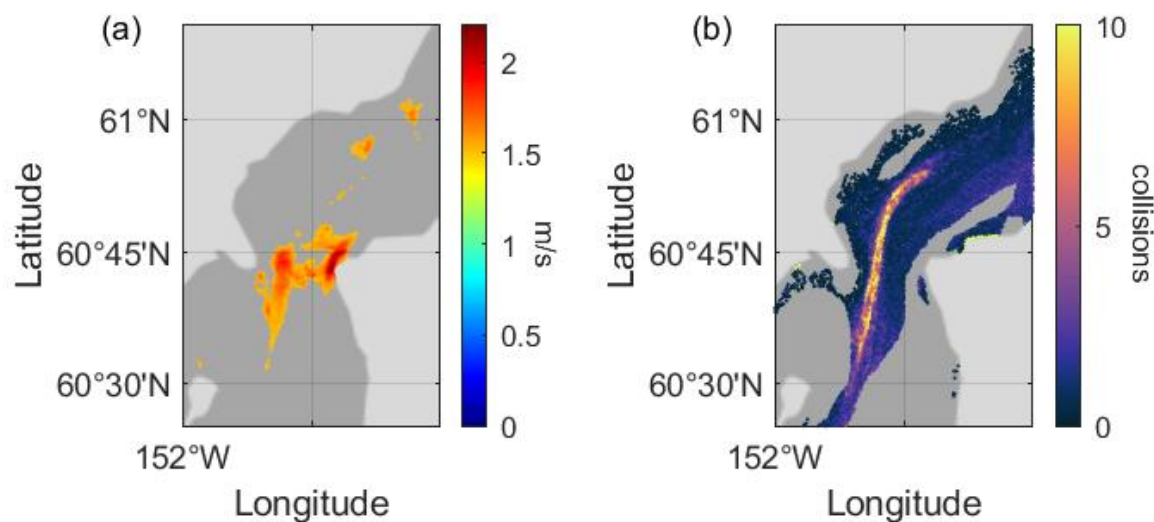
Figure 15.   Comparison of high current speed locations with collision risk. (a) Locations where the depth- and time-averaged current speeds output by the FVCOM model are >1.5 m/s. (b) Maximum collisions of Runs 8-11 where the average February sea ice concentration is >30%.
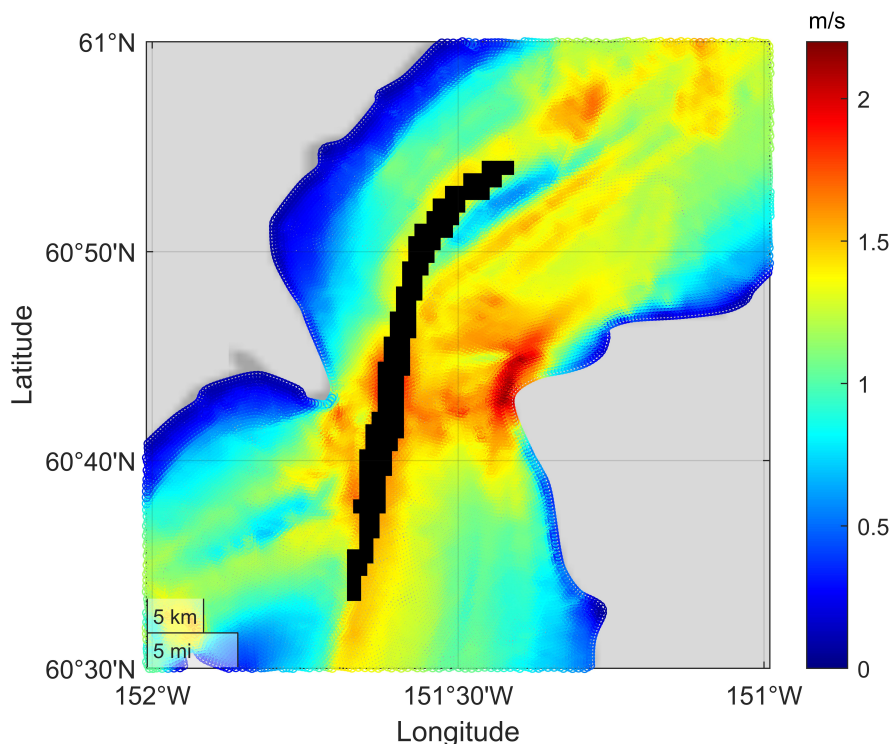
Figure 16.   Current speed map for turbine siting in the Forelands region with the high collision risk area marked in black. The current speed data are depth and time averaged over the FVCOM run. The black collision risk area shows locations where the maximum collisions were greater than five and the average February sea ice concentration was greater than 30%.

4.0   Conclusions and Recommendations

The combination of a hydrodynamic model, a trajectory model, and remotely sensed sea ice concentration data has identified areas in Cook Inlet that would be preferable for turbine siting and areas that have high risks of sea ice collisions. The trajectory modeling revealed that many particles travel through one area in the west Foreland region. The trajectories are concentrated in that area as the ice particles are moved south by the prevailing winds. This thin strip is an area with high current speeds, which makes it a good location for turbines, but it is also a region with significant sea ice. This implies the sea ice collision risk at the surface is high and that area should be avoided as a turbine site if other sites have comparable current speed characteristics. An area closer to the east Forelands region also has high current speeds but has lower sea ice concentrations and fewer particle trajectories that transit through the area. The area close to the east Forelands has the added advantage of being close to the power grid in Nikiski. The combination of high current speeds, low collision risk, and proximity to the power grid make the east Forelands the preferred site.

The model runs documented in this report give the first estimate of a map of collision risks in Cook Inlet. To improve the accuracy of estimates of collision risk, river flow, estuarine circulation induced by salinity and temperature gradients, and wave action should be simulated. The FVCOM model could also be run for longer time periods so that the run coincides with different sea ice conditions. Longer time periods would explore the variability of the wind conditions during different months of the sea ice season. Wind had a strong influence on the particle trajectories and therefore the estimated collision risk. It is important to understand the wind variability during the months when sea ice is present in order to accurately predict particle trajectories and predict collision risks. The collision risk assessment approach used in this study is not only useful for turbine siting, but is also applicable to other offshore structures such as oil platforms or wind turbines. Future studies may use this approach to study different sites in sea ice-affected areas before offshore structures are installed.

References

Beegle-Krause, C. (1999), Gnome: Noaa's next-generation spill trajectory model, in *Oceans' 99. MTS/IEEE. Riding the Crest into the 21st Century. Conference and Exhibition. Conference Proceedings (IEEE Cat. No. 99CH37008)*, vol. 3, pp. 1262–1266, IEEE.

Beitsch, A., L. Kaleschke, and S. Kern (2014), Investigating high-resolution amsr2 sea ice concentrations during the february 2013 fracture event in the beaufort sea, *Remote Sensing*, *6*(5), 3841–3856.

Chen, C., H. Liu, and R. C. Beardsley (2003), An unstructured grid, finite-volume, three-dimensional, primitive equations ocean model: application to coastal ocean and estuaries, *Journal of atmospheric and oceanic technology*, *20*(1), 159–186.

Chen, C., R. C. Beardsley, and G. Cowles (2006), An unstructured grid, finite-volume coastal ocean model (fvcom) system, *Oceanography*, *19*(1), 78.

Huang, S., M. Huang, Y. Lyu, and L. Xiu (2021), Effect of sea ice on seismic collapse-resistance performance of wind turbine tower based on a simplified calculation model, *Engineering structures*, *227*, 111,426.

Johnson, M. (2008), Water and ice dynamics in cook inlet, *Tech. rep.*, University of Alaska Fairbanks.

Kaleschke, L., C. Lüpkes, T. Vihma, J. Haarpaintner, A. Bochert, J. Hartmann, and G. Heygster (2001), Ssm/i sea ice remote sensing for mesoscale ocean-atmosphere interaction analysis, *Canadian journal of remote sensing*, *27*(5), 526–537.

Kilcher, L., R. Thresher, and H. Tinnesand (2016), Marine hydrokinetic energy site identification and ranking methodology part ii: tidal energy, *Tech. rep.*, National Renewable Energy Lab.(NREL), Golden, CO (United States).

Maximenko, N., J. Hafner, M. Kamachi, and A. MacFadyen (2018), Numerical simulations of debris drift from the great japan tsunami of 2011 and their verification with observational reports, *Marine pollution bulletin*, *132*, 5–25.

Mulherin, N. D., W. B. Tucker III, O. P. Smith, and W. J. Lee (2001), Marine ice atlas for cook inlet, alaska, *Tech. rep.*, Engineer Research and Development Center Hanover NH Cold Regions Research.

NOAA (2013), Severe marine debris even report: Japan tsunami marine debris, *Tech. rep.*

Parker, D., and J. Jacobs (2018), Cook inlet ice guidelines: A best practice for stakeholder engagement, *Coast Guard Journal of Safety & Security at Sea, Proceedings of the Marine Safety & Security Council*, *75*(2).

Sanderson, B. G., and A. M. Redden (2015), Perspective on the risk that sediment-laden ice poses to in-stream tidal turbines in minas passage, bay of fundy, *International Journal of Marine Energy*, *10*, 52–69.

Wang, T., and Z. Yang (2020), A tidal hydrodynamic model for cook inlet, alaska, to support tidal energy resource characterization, *Journal of Marine Science and Engineering*, *8*(4), 254.

**Pacific Northwest
National Laboratory**

902 Battelle Boulevard
P.O. Box 999
Richland, WA 99352
1-888-375-PNNL (7675)

www.pnnl.gov